

Confined Magneto-Optical Waves in Graphene

Aires Ferreira,^{1,2} N. M. R. Peres,^{1,2} and A. H. Castro Neto¹

¹*Graphene Research Centre and Department of Physics,
National University of Singapore, 2 Science Drive 3, Singapore 117542*

²*Department of Physics and Center of Physics, University of Minho, P-4710-057, Braga, Portugal*

The electromagnetic mode spectrum of single layer graphene subjected to a quantizing magnetic field is computed taking into account intraband and interband contributions to the magneto-optical conductivity. We find that a sequence of weakly decaying *quasi*-transverse electric modes, separated by magnetoplasmon polariton modes, emerge due to the quantizing magnetic field. The characteristics of these modes are tuneable, by changing the magnetic field or the Fermi energy.

PACS numbers:

I. INTRODUCTION

The field of plasmonics has been considered the photonics milestone of the year 1998. To this choice contributed the landmark paper of Ebbesen *et al.* on the “extraordinary optical transmission through sub-wavelength hole-arrays”. [1] The effect was explained on the basis of the properties of surface-plasmon polaritons. [2]

Surface-plasmon polaritons (SPP) are electromagnetic surface-waves, guided by a metallic interface, resulting from the coupling of the electromagnetic field to the collective plasma excitations of the metal. [2] These guided modes are of important in fields as different as light guides at the nanoscale, [3] spectroscopy and sensing, enhancement of light absorption in solar cells, enhanced Raman spectroscopy, and others.

Graphene, being an one atom-thick metallic film is an obvious candidate for investigations on SPP. Recent research has established plasmon-based enhanced Raman spectroscopy and photocurrent, [4, 5] as well as room temperature prominent absorption peaks in the terahertz spectral range, [6] and nanoscopy of mid-infrared radiation confinement. [7]

Both in the two-dimensional (2D) electron gas and in graphene, the plasmon dispersion has a square-root dependence on the wave vector: $\Omega_{2D}(\mathbf{q}) \propto \sqrt{q}$. The linear dispersion of the electrons in graphene, $\epsilon(\mathbf{q}) = \pm v_F q$, where v_F is the Fermi velocity, implies that $\Omega_{2D}(\mathbf{q}) \propto \sqrt{k_F q}$, where $k_F \propto \sqrt{n_e}$ is the Fermi momentum and n_e is the electronic density. [8] If a grid of period L is superimposed on graphene, plasmons of wave number $q \sim 1/L$ can be excited. [2, 9] Furthermore, since $\Omega_{2D}(\mathbf{q}) \propto \sqrt{k_F q}$, we expect the scaling relation $\Omega_{2D}(\mathbf{q}) \propto n_e^{1/4} L^{-1/2}$, which has been observed experimentally. [6]

Graphene has a number of advantages over other metallic thin films used in plasmonics; e.g., the ability of changing its carrier concentration using a gate, allowing a fine control over the frequency range for plasmonic excitations, [7] and long propagation lengths as compared to conventional SPP. [10, 11] Furthermore, inhomogeneous doping in a single graphene sheet allows

the drawing of SPP propagation paths. [3]

When an external magnetic field perpendicular to a 2D electron gas is applied, hybridization between cyclotron excitations and plasmons occurs originating magnetoplasmon modes. [12, 13] The presence of the magnetic field gives rise to strong absorption peaks making the dispersion of electromagnetic modes very sensitive to the frequency. In the present work, we demonstrate that in addition to magnetoplasmon polaritons (MPP), graphene supports extremely weakly damped modes, which due to their resemblance to conventional transverse electric modes, are here referred to as *quasi*-transverse electric (QTE). This article is organized as follows; in Sec. II we overview the dispersion relation of electromagnetic modes supported by 2D electron systems. We revisit the simpler problem of zero external field, for which two types of modes can exist: SPP and weakly damped modes (transverse electric) with characteristics similar to photons propagating in a dielectric. The magneto-optical response of graphene in the presence of a quantizing magnetic field is described in Sec. III. The full mode dispersion is calculated in the presence of disorder by employing the optical limit approximation to the conductivity. The losses, confinement, and polarization of the solutions are studied carefully. The outlook and conclusions are presented in Sec. IV. Technical details and derivations are given in appendices.

II. DISPERSION RELATION

We consider an infinite graphene film in the xy plane embedded in a dielectric medium of permittivity (permeability) ϵ (μ). [14] A static quantizing magnetic field is applied along the transverse (z) direction. We focus on electromagnetic modes propagating along the x axis,

$$\mathbf{E}(\mathbf{r}, t) = \mathbf{E}_0 e^{i(qx - \omega t)} e^{-\kappa|z|}. \quad (1)$$

The symbols have the usual meanings: ω denotes the angular frequency, q is the complex longitudinal wavevector and κ encodes the amount of confinement along the transverse direction. Maxwell equations relate these quanti-

ties according to the general relation $q^2 = \kappa^2 + \epsilon\mu\omega^2$, so that in general both q and κ are complex quantities. Note that a similar equation holds for the magnetic field $\mathbf{H}(\mathbf{r}, t)$. Throughout, we employ SI units and the notation $z = z' + iz''$ for complex variables.

The dispersion relation of electromagnetic modes follows from the boundary conditions for the fields at the interface $z = 0$, [12]

$$\det \left(\begin{array}{cc} \frac{i\kappa\sigma_L(q,\omega,B)}{2\epsilon\omega} + 1 & \frac{\mathcal{Z}}{2}\sigma_H(q,\omega,B) \\ \frac{\mathcal{Z}}{2}\sigma_H(q,\omega,B) & \frac{i\mu\omega\sigma_L(q,\omega,B)}{2\kappa} - 1 \end{array} \right) = 0, \quad (2)$$

where B is the intensity of the magnetic field, $\mathcal{Z} = \sqrt{\mu/\epsilon}$ is the impedance of the surrounding medium and σ_L (σ_H) denotes the longitudinal (Hall) conductivity of graphene. The physical solutions of the above equation, $\omega \equiv \Omega(q)$, contain the full mode spectrum of the system—a derivation of the dispersion relation is given in Appendix A. The characteristics of the mode spectrum are determined by the conductivity tensor. The latter depends on q , ω , B , and, generally, also on the Fermi energy E_F , temperature and sample-specific broadening parameters. In the present work, we neglect the dependence of $\sigma_{L(H)}$ on the in-plane wavevector q , and thus, hereafter, $\sigma_{H(L)}$ denotes the optical (local) limit of the dynamical conductivity, i.e., $\sigma_{H(L)} \equiv \sigma_{H(L)}(\omega, B) = \sigma_{H(L)}(0, \omega, B)$. The latter is justified for small wavevectors, more precisely for $ql_B \ll 1$, where $l_B = \sqrt{\hbar/eB}$ denotes the magnetic length ($-e < 0$ is the electron charge).

In the absence of an external field B , the solutions of Eq. (2) are the so-called transverse electric and transverse magnetic modes, namely, $\kappa = i\Omega\mu\sigma_L(\Omega, 0)/2$ and $\kappa = 2i\Omega\epsilon/\sigma_L(\Omega, 0)$, respectively. In the former, the electric field is perpendicular to the direction of propagation, the mode dispersion is close to the light line, $\Omega \simeq cq'$, and damping is small ($q'', \kappa' \ll q'$). Transverse electric modes require a negative reactive conductivity, $\sigma_L''(\omega, 0) < 0$, and hence are not observed in conventional 2D gases (we note that when $\sigma_L'' < 0$ and $\sigma_L'/|\sigma_L''| \ll 1$ the behavior of the system resembles that of a dielectric). On the other hand, transverse magnetic waves are confined to the metallic surface, featuring large field localization, thus having important applications in sub-wavelength optics and plasmonics.[15] In graphene both modes can exist because near at interband threshold, $\omega = 2E_F/\hbar$, the function $\sigma_L''(\omega, 0)$ changes sign.[16] Coupling and guiding of transverse electric modes by graphene in zero-field have been recently reported in Ref. 17.

III. MAGNETO-OPTICAL MODES

When a magnetic field is turned on, electrons acquire considerable cyclotronic energies via the Lorentz force, and at sufficiently high fields, the continuum Dirac quasiparticle spectrum condensates into Landau levels (LLs)

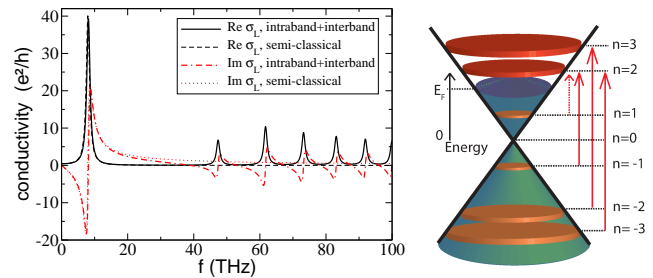


Figure 1: Doped graphene in a magnetic field of 5 T at zero temperature ($E_F = 0.1$ eV). **Left:** σ_L is plotted as a function of the frequency $f = \omega/2\pi$. Clearly, $\sigma_L'' < 0$ in various frequency intervals. The full quantum calculation is seen to be crucial above ~ 20 THz. **Right:** The first few electronic transitions are shown. The Fermi energy lies slightly above the Landau level with $n = 1$, and thus only transitions to levels with $n \geq 2$ are allowed. The (small) dashed arrow stands for the intraband transition responsible for the strong peak observed near at 7.8 THz. Other arrows represent interband transitions.

[Fig. 1 (right panel)]. In order to investigate how the zero-field picture changes due to the quantizing magnetic field, we employ linear-response theory within the Dirac cone approximation to obtain an expression for $\sigma_{L(H)}(\omega, B)$ with both intraband and interband contributions included. (See Appendix B.)

The main features of $\sigma_L(\omega, B)$ for doped graphene in a quantizing field are shown in Fig. 1 (left panel) for frequencies up to the near-infrared. As a figure of merit, we choose $E_F = 0.1$ eV and field intensity $B = 5$ T, both being typical values used in experiments. $\sigma_L(\omega, B)$ consists of an intraband term with spectral weight located at the lower-end of the spectrum (the strong peak at $f \simeq 8$ THz), and interband high-frequency contributions originating a series of peaks above the interband threshold $f \simeq 43$ THz. The position and shape of each of these peaks depend on the particular values of E_F and B , but the main qualitative features in Fig. 1 are general. For a comprehensive discussion of the magneto-optical response of graphene see Refs. 18, 19.

In order to account for disorder, we have used an energy-independent LL broadening of $\Gamma = 2.5$ meV (and also $\Gamma = 10$ meV in one figure) in consistency with the values found in pump-probe experiments performed in epitaxial and exfoliated graphene samples,[20, 21] and on infrared spectroscopy studies of the Drude conductivity of graphene.[22] The renormalization of the optical conductivity due to the electron-phonon interactions is neglected. From the studies of magneto density of states taking into account the E_{2g} optical mode at 200 meV,[23] we expect the latter approximation to be valid in the entire range of frequencies considered here.

In 2D electron gases, plasmons and cyclotronic excitations (with frequency ω_c) hybridize leading to the well-known semi-classical magnetoplasmon spectrum, $\Omega^2 =$

$\Omega_{2D}^2 + \omega_c^2$. [12, 13] In view of the strong contribution of interband transitions to σ_L'' (e.g., see the discrepancy between the semi-classical calculation and the quantum formula, even at low frequencies, in the left panel of Fig. 1), this formula should be of limited applicability in graphene. Moreover, Shubnikov–de Haas oscillations originate many frequency regions with $\sigma_L'' < 0$, and hence, similarly to 2D magnetized electron Fermi gas, [12, 24] we may expect the splitting of the mode spectrum into many branches.

In what follows, unless stated otherwise, we refer to the particular system in Fig. 1. We complement the discussion with analytic expressions that can be used to compute the several quantities for general parameters. The full mode spectrum is presented in Fig. 2; only non-exponentially growing solutions of Eq. (2) are shown ($\kappa' \geq 0$). The most notorious feature is the existence of a series of well-defined branches, labeled by the integers $n = 1, 2, \dots$, etc. These branches can be divided into two distinct sets, namely, the set of branches with dispersion close to the light line (n odd) and the remaining (n even). The former will be shown to have the basic properties of transverse electric modes and hence are termed QTE, whereas the latter are MPP modes (with polarization not necessarily similar to transverse magnetic modes due to the applied magnetic field).

Our results borne out two peculiar features of graphene: i) n even branches have two distinct solutions for each wavevector q' . This degeneracy is a result of hybridization between even and odd modes (see below), and ii) the frequency domain size of each branch is non-uniform due to the structure of LLs in graphene. The first branch occupies a region $[0, f_1[$, the second $[f_1, f_2[$, etc., where f_n is defined to be the n -th node of the reactive longitudinal conductivity, $\sigma_L''(2\pi f_n, B) = 0$. For the system under discussion, the nodes read $f_1 \simeq 8$ THz, $f_2 \simeq 39$ THz, etc.

Let us now discuss with detail the region $f \lesssim 20$ THz spanning two branches, $n = 1, 2$. Here, the magneto-optical transport is predominantly semi-classical (see Fig. 1), and hence the relevant frequency scale is the cyclotron frequency, $\omega_c = ev_F^2 B / |E_F|$ ($v_F \simeq 10^6$ m/s is Fermi velocity of carriers in graphene). At $f < f_1$, the dispersion curve is pinned to the light dispersion line, $\Omega(q') \simeq cq'$, except for frequencies very close to f_1 , where the dispersion curve shifts slightly towards the left-hand side (see inset) and part of the transverse electric character is lost. The latter signals the onset of a rapid increase of σ_L'' , as a result of a strong absorption peak at $f_1 \simeq \omega_c / 2\pi$ (Fig. 1). Last, when f becomes larger than f_1 , σ_L'' changes sign, and a MPP branch develops. This mode displays the strong confinement to the 2D interface ($\kappa' \sim q'$) that characterizes conventional transverse magnetic modes. Its polarization varies significantly with frequency/wavevector as shown later.

The simultaneous presence of the two distinct branches

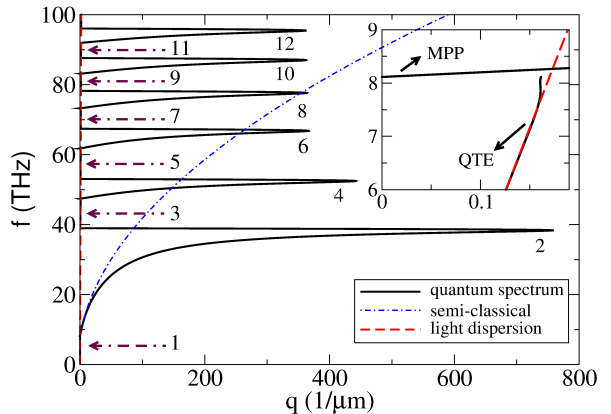


Figure 2: Mode frequency $f = \Omega/2\pi$ for doped graphene in a field of 5 T is plotted as a function of the longitudinal momentum q' [solid (black) line]. For completeness, the light dispersion, $f = cq'/2\pi$ is shown by the dashed (red) line, and the semi-classical solution is given by the dashed-dotted (blue) line. Inset: Mode spectrum near zero momentum. Arrows in the main panel indicate QTE solutions and numbers identify the distinct branches. Other parameters as in Fig. 1.

($n = 1, 2$) in the intraband region can only occur for sufficiently high fields, $B > B_c \equiv |E_F| \Gamma / e\hbar v_F^2$, otherwise one obtains a single type of solution with plasmon character, $\Omega(q') \sim \sqrt{q'}$, as for $B = 0$. [25, 26] The reason is that for $B < B_c$ the reactive part of the conductivity is always positive below the interband threshold, forbidding the existence of modes with dispersion close to the light line (QTE modes) in the low-frequency region. The transition frequency Ω (at which the MPP $n = 2$ mode begins) is given by the solution of Eq. (2) with $q' = 0$, [27]

$$\Omega(0) \approx \sqrt{\omega_c^2 - \Gamma^2/\hbar^2}, \quad (3)$$

Using the above expression, we obtain $\Omega(0) \approx 2\pi \cdot 8$ THz in good agreement with the numerical result (see inset in Fig. 2).

The semi-classical expression for the MPP dispersion $\Omega_{(\text{MPP})}(q')$ can be derived assuming $T = 0$ and ignoring the interband contributions to the magneto-optical conductivity,

$$\Omega_{(\text{MPP})}(q') \simeq \sqrt{[\Omega_{2D}(q')]^2 + \omega_c^2}, \quad (4)$$

where $\Omega_{2D}(q') = (e/\hbar)\sqrt{q'|E_F|/(2\pi\epsilon)}$ is the graphene's longitudinal plasmon dispersion in zero field. The above expression is valid for $q' \gg \Omega/c$, and for Ω within the regime of validity of the semi-classical transport theory, $\Omega \ll 2E_F/\hbar$ (see dotted-dashed line in the main panel of Fig. 2). Eq. (4) predicts an increase of MPP's frequency due to the presence of a magnetic field. A derivation of the above formula is given in Appendix C. This result coincides semi-classical magnetoplasmon spectrum for a 2D electron gas. [12, 13]

We now turn our attention to the mid/near-infrared part of the spectrum, where new branches ($n = 3, 4, \dots$)

emerge due to interband transitions. Figure 2 shows that the quantum calculation (solid line) deviates considerably from the semi-classical result already at $f \approx 20$ THz. In particular, the quantum corrections cause a considerable slow down of the MPP's group velocity, $v_g = \partial_{q'}\Omega(q')$, relative to its semi-classical value. This effect comes from the superposition of interband resonances tails that contribute with substantial weight even well below the interband threshold. For instance, in the range $f \approx [20, 30]$ THz, the interband terms yield a correction to the conductivity of about $\sim 0.5ie^2/h$ (see Fig. 1) explaining the bending of the solid curve relatively to the dashed-dotted curve in Fig. 2. Near at $f = f_2 \approx 40$ THz, σ_L'' changes sign again, and a large bandwidth (≈ 10 THz) QTE mode develops. The first six QTE modes are indicated by arrows in Fig. 2. Their dispersion relation is well approximated by $\Omega(q') \simeq cq'$, except within the QTE/MPP crossovers ($f \simeq f_n$, with n odd), where $\Omega(q')$ acquires a complex form due the strong variation of the optical properties induced by sharp absorption peaks in these regions.

The full dispersion relation for the MPP branches is rather cumbersome because, as noted above, many interband terms contribute to the spectral weight around a particular frequency; see Eq. (20) and text therein. A compact expression for $q(\omega)$ valid for every MPP branch can still be obtained by considering $T = 0$ and neglecting the Hall conductivity term in Eq. (2). These approximations are justified since i) for a quantizing magnetic field, the conductivity of graphene does not vary significantly with temperature, and ii) σ_H can be shown to provide a small correction only in the vicinity of each f_n . We obtain,

$$\sqrt{q^2 - \epsilon\mu\omega^2} \simeq \frac{i\epsilon\omega h}{e^2} \left(\frac{\Gamma/E_1(B)}{1 - i\hbar\omega/\Gamma} \right) \Psi^{-1}(\omega, B), \quad (5)$$

$$\Psi(\omega, B) = \sum_{n=|N_F|}^{N_{\text{cut}}'} \frac{E_1(B)/\Delta_n(B)}{(1 - i\hbar\omega/\Gamma)^2 + \Delta_n(B)^2/\Gamma^2}. \quad (6)$$

In these expressions, $E_n(B) = s_n\sqrt{2|n|}\hbar v_F/l_B$ [where $s_n \equiv \text{sign}(n)$] is the energy of the n -th (degenerate) LL in graphene, $N_F = \text{int}[(E_F/E_1(B))^2] \geq 0$ is the number of occupied(empty) electron(hole) degenerate LLs with $|E_n| > 0$, and $\Delta_n(B)$ is the n -th interband resonance energy, defined as $\Delta_n(B) \equiv E_{n+1}(B) + E_n(B)$. The prime in the summation sign indicates that if $N_F \neq 0$ the first term is to be halved. Also, a cutoff $n \leq N_{\text{cut}}$ must be taken when computing this summation (see Appendix B). For simplicity, the above expression for $\Psi(B, \omega)$ only includes the interband contribution to σ_L . The inclusion of the intraband spectral weight [see Eq. (24)] in $\Psi(B, \omega)$ is straightforward and plays a role only in the first MPP branch. Figure 3 shows that the MPP spectrum computed from Eq. (5) cannot be distinguished from the full calculation. The latter agreement extends down to low

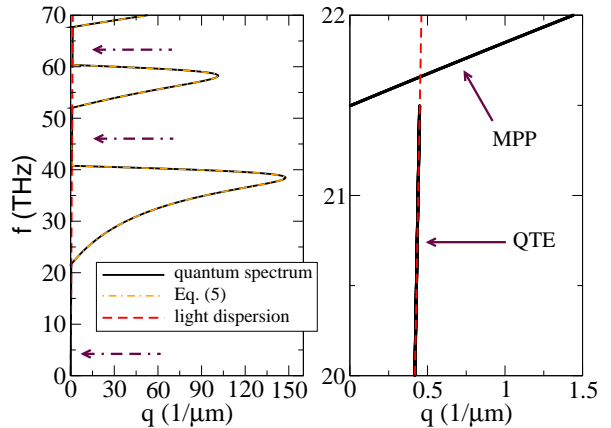


Figure 3: Mode frequency for doped graphene ($E_F = 0.05$ eV) in a field of 6 T as a function of q' [solid (black) line]. The broadening reads $\Gamma = 10$ meV. Arrows in the left panel indicate the first three QTE modes.

frequency (the first MPP branch) because in the system plotted in Fig. 3 all electrons (and holes) occupy the zero energy state, that is, $N_F = 0$. Indeed, according to our definition of interband and intraband contributions to the conductivity when $N_F = 0$ (see Appendix B), $\Psi(B, \omega)$ already contains the full spectral weight in this case.

We have discussed the general features of the mode spectrum of graphene under a quantizing electromagnetic field. It has been shown to consist of several branches, each possessing two distinct types of modes. In what follows, we demonstrate that MPP solutions have conventional decaying properties of SPP, whereas the QTE modes are essentially non-decaying, with electric field nearly transverse (hence their name). The MPP solutions will be shown to have a rich polarization diagram with longitudinal (transverse magnetic) character only emerging at specific frequency intervals.

Decaying and polarization properties

The decaying properties of the modes are summarized in Fig. 4. QTE modes display large localization length in x [z] direction, namely, q''/q' [κ'/q'] in the range 10^{-9} - 10^{-2} [10^{-6} - 10^{-1}] (see for instance the first branch; top left panel). MPP modes, on the other hand, always show considerable decay along the z direction, $\kappa' = \mathcal{O}(q')$, indicating strong confinement. The losses in the propagation direction x , on the other hand, vary appreciably and are determined by the graphene's absorption at the specific MPP frequency; e.g., in the range 8-20 THz, the longitudinal decay rate q'' varies in the range $0.1q'$ - $100q'$, with maximum loss occurring near at the cyclotron frequency ($\simeq 8$ THz).

Although the losses and confinement reported here have orders of magnitude comparable to those in the ab-

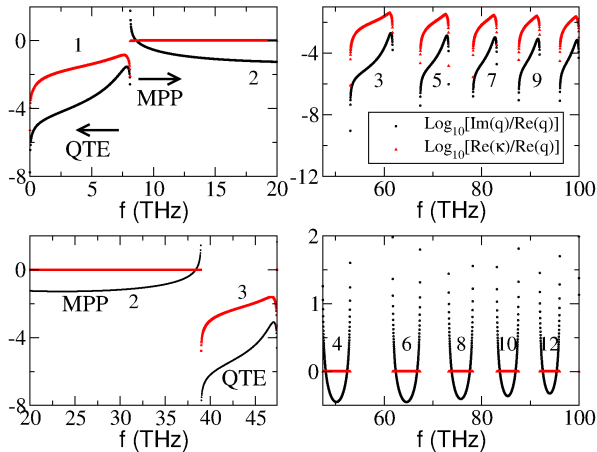


Figure 4: The ratios q''/q' and κ'/q' , which characterize the longitudinal and transverse decaying rates, respectively, are plotted in logarithmic scale as a function of the mode frequency. Several panels are given to help visualize the difference between QTE and MPP modes. (System parameters as in Fig. 1.)

sence of a magnetic field[10], the strong dependence of these quantities on the frequency is exclusive to the 2D interface subjected to a strong external magnetic field (Fig. 4 shows that the decay characteristics can vary by several orders of magnitude around at $f = f_n$ for all n). An important effect of the magnetic field is to allow for QTE modes with lower losses than the zero-field transverse electric mode in specific frequency intervals; for instance, above 50 THz, q''/q' can reach a minimum value of the order of 10^{-7} , whereas for $B = 0$ (and other parameters unchanged) this ratio is about $\sim 10^{-5}$ in the frequency window 50-100 THz.

In order to complete our study, we demonstrate that the electric field of QTE modes are essentially transverse and study how the longitudinal (transverse magnetic) character of MPP modes depend on the wavevector. To this end, we compute the ratios $\mathcal{E}_{xy(zy)} \equiv E_{x(z)}/E_y$ and $\mathcal{B}_{xy(zy)} \equiv B_{x(z)}/B_y$. From Maxwell equations, we easily obtain,

$$\mathcal{E}_{xy} = \left(\sigma_L - \frac{1}{i\omega} \frac{2\kappa}{\mu} \right) / \sigma_H, \quad (7)$$

$$\mathcal{B}_{xy} = i \frac{\kappa}{\omega} \left(2 - \frac{\kappa}{i\omega\epsilon} \sigma_L \right) / \mu \sigma_H, \quad (8)$$

and $\mathcal{E}(\mathcal{B})_{zy} = \mathcal{E}(\mathcal{B})_{xy} \times iq/\kappa$, where it is assumed $B > 0$ so that $\sigma_H \neq 0$. These quantities are plotted in the bottom panel of Fig. 4 for a frequency range spanning the $n = 1$ and $n = 2$ branches. Below 8 THz, the electric components ratios $\mathcal{E}_{xy(zy)}$ (plotted in the right panel) are found to have magnitude in the range 10^{-3} - 10^{-2} (10^{-2} - 10^{-1}), confirming that the electric field of QTE modes lies prominently along the y axis, resembling pure transverse electric modes [which have $\mathcal{E}_{xy(zy)} = 0$]. The magnetic ratios of these modes are shown in the left panel.

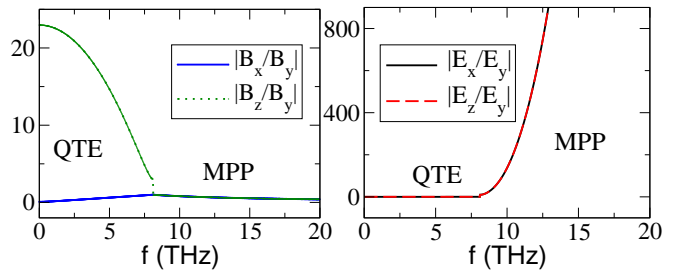


Figure 5: Polarization properties of the electromagnetic modes within the first two branches. The left panel shows the complex modulus of the magnetic ratios \mathcal{B}_{xy} and \mathcal{B}_{zy} , whereas the respective electric counterpart, \mathcal{E}_{xy} and \mathcal{E}_{zy} , are given in the right panel. (System parameters as in Fig. 1.)

As for the MPP branch, we find magnetic ratios $\mathcal{B}_{xy} \simeq \mathcal{B}_{zy}$ in the range 0.5-1, and hence the polarization of these modes are distinct from transverse magnetic modes (which have $\mathcal{B}_{xy(zy)} = 0$). In this MPP branch, the magnetic ratio \mathcal{B}_{xy} decreases with increasing frequency/ q' with a minimum (not shown) occurring at 34 THz, $\mathcal{B}_{xy} \simeq 0.05$. The latter signals the beginning of a crossover to a QTE branch: the longitudinal character is lost (\mathcal{B}_{xy} increases) as the turning point (maximum q') is approached. Similar conclusions can be drawn for the remaining branches.

The situation described in the above paragraph is distinct from 2D electron gases,[12, 24] where solutions become more longitudinal with increasing wavevector. A question that deserves further investigation is whether the effect of finite $\mathbf{q} = q'\mathbf{e}_x$ in σ_L can influence the solutions at large q' . Note that $l_B = \mathcal{O}(10^{-8}B^{-1/2})$, with B in Tesla, and hence a considerable renormalization of spectrum is expected for the largest wavevectors discussed here, specially in Fig. 2 where q' can be as large as $8 \times 10^8 \text{ m}^{-1}$. The lack of longitudinal character of MPP at large q' reported here may indeed result from an inadequacy of the optical limit in describing that region of the spectrum. On the other hand, the system represented in Fig. 3 ($B = 6 \text{ T}$ and $\Gamma = 10 \text{ meV}$) displays modes with smaller wavevectors, making the optical limit less restrictive in this case. Notwithstanding, similar features are observed in this system, thus providing further evidence for the generality of the phenomena discussed in this article (QTE-MPP crossovers, degeneracy of MPP branches, etc.).

MPP wave localization

We briefly address the wave localization characteristics of the MPP waves reported here. It is a well established fact that SPP in a metal can have wavelengths considerably smaller than electromagnetic waves of the same frequency in a dielectric.[15] In graphene in zero

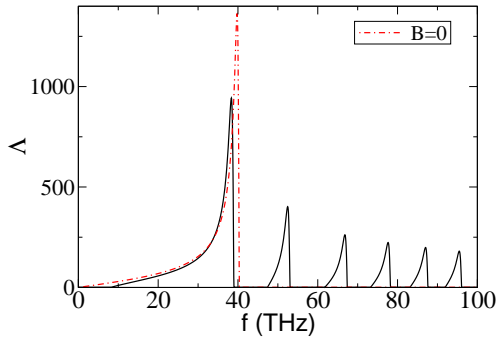


Figure 6: The wave localization ratio Λ is plotted as a function of the mode's frequency for a magnetic field of 5 T. The dashed-dotted (red) line shows the result for $B = 0$ for comparison. Other parameters as in Fig. 1.

field this shrinkage effect is enhanced when compared to conventional 2D electron gas SPP.[10, 11] Figure 6 shows the ratio of the wavelength in vacuum to the MPP mode wavelength, $\Lambda = \lambda_0/\lambda$ (here, $\lambda_0 = 2\pi c/\omega$ and $\lambda = 2\pi/q'$). It can be seen that for 5 T, below the interband threshold, Λ is comparable to that obtained in the case of zero field. In particular, near the frequency resonant to the $n = -1 \rightarrow n = 2$ interband transition (see also Fig. 1), we obtain a large peak of about $\Lambda \sim 10^3$, a figure comparable to the $B = 0$ scenario (see how the peaks compare in Fig. 6). The remaining MPP modes in that figure show peaks with $\Lambda \sim 10^2$. QTE solutions, on the other hand, have $\Lambda \simeq 1$ regardless their frequency, a characteristic of transverse electric modes.

A simple formula for Λ can be obtained in the intraband region; using Eq. (4) we obtain

$$\Lambda \approx \frac{1}{2\alpha_g E_F} \left(\hbar\Omega - \frac{[\Delta(B)]^2}{\hbar\Omega} \right), \quad (9)$$

where $\alpha_g = e^2/(4\pi\epsilon\hbar c)$ denotes the graphene's fine structure constant and $\Delta(B) = \hbar v_F^2 B/E_F$ is the cyclotron energy. The above expression predicts a decrease of Λ with the magnetic field, which is consistent with the curves reported in Fig. 6 in the region where Eq. (4) [and hence Eq. (9)] is valid, i.e., 8-20 THz. In the limit of $B \rightarrow 0$, Eq. (9) reproduces the result reported in Ref. [11].

IV. OUTLOOK AND CONCLUSIONS

We have computed the mode spectrum of electromagnetic modes supported by a graphene interface in the presence of a quantizing magnetic field. We have found a rich structure with extended crossovers between *quasi*-transverse electric (QTE) and magnetoplasmon polariton (MPP) modes as a consequence of characteristic Shubnikov-de Haas oscillations in the magneto-optical response of graphene. Analogously to the 2D Fermi gas, the dispersion relation splits in a large number of

branches.[12, 24] Interband transitions between the bottom and top Dirac cones originate terms in the conductivity with considerable spectral weight in the semi-classical (low-frequency) region. As a consequence, the conventional semi-classical 2D magnetoplasmon dispersion becomes restricted to a narrow wavevector/frequency interval. Our calculation within the optical limit approximation to the conductivity predicts that, unlike 2D Fermi gases, each MPP mode with a given wavevector admits two possible values of frequency. The consequences of a non-zero wavevector \mathbf{q} in the conductivity for the QTE-MPP spectrum is a challenging question and deserves further investigation.

In summary, we have shown that a quantizing magnetic field changes the conventional picture of electromagnetic modes in graphene.[10, 16] In the LL regime, we predicted a series of branches in the mode spectrum, consisting of magnetoplasmon polaritons and *quasi* transverse electric modes. At small frequencies, a QTE persists, even in the semi-classical regime, as long as the cyclotronic frequency is larger than the electrons relaxation's rate. Due to the high LL energy gaps, these effects should be observable up to room temperature.

V. ACKNOWLEDGEMENTS

This work was supported by the NRF-CRP award "Novel 2D materials with tailored properties: beyond graphene" (R-144-000-295-281).

VI. APPENDIX A: MODE SPECTRUM

For our purposes it is sufficient to consider a single Fourier component of the electromagnetic field in the following form

$$\mathbf{E}_m = (E_{m,x}, E_{m,y}, E_{m,z}) e^{i(q_m x - \omega t)} e^{-\kappa_m |z|}, \quad (10)$$

where κ_m accounts for possible attenuation in the transverse direction to graphene. The subscript $m = 1(2)$ denotes the region of space with $z > 0(z < 0)$. Here, we consider the more general case of graphene embedded in dielectric mediums with permittivities ϵ_1 and ϵ_2 .

We require $\kappa'_m \geq 0$ and $q''_m/q'_m \geq 0$. The former means that the wave can be confined to the z plane and must not diverge as $z \rightarrow \pm\infty$, whereas the second condition allows wave attenuation as it propagates in the graphene plane (the formal divergence at $x \rightarrow -\infty$ is a consequence of the beginning of the perturbation at $t = -\infty$).

Macroscopic Maxwell equations imply the following relation between the field amplitudes,

$$i\omega \vec{\mathcal{F}}_m = M_m \vec{\mathcal{F}}_m, \quad (11)$$

where $\vec{\mathcal{F}}_m$ is the six-dimensional vector of amplitudes $\vec{\mathcal{F}}_m = (\mathbf{E}_m, \mathbf{B}_m)$ and,

$$M_m = \begin{bmatrix} 0 & M_{m,R} \\ M_{m,L} & 0 \end{bmatrix}, \quad (12)$$

with

$$M_{m,R} = \frac{1}{\epsilon_m \mu_m} \begin{bmatrix} 0 & (-1)^m \kappa_m & 0 \\ (-1)^{m+1} \kappa_m & 0 & i q_m \\ 0 & -i q_m & 0 \end{bmatrix}, \quad (13)$$

$$M_{m,L} = \begin{bmatrix} 0 & (-1)^{m+1} \kappa_m & 0 \\ (-1)^m \kappa_m & 0 & -i q_m \\ 0 & i q_m & 0 \end{bmatrix}. \quad (14)$$

A straightforward consequence of Eq. (11) is the well-known relation,

$$q_m^2 = \kappa_m^2 + \epsilon_m \mu_m \omega^2. \quad (15)$$

The mode spectrum for this problem is derived by imposing the boundary conditions for the electromagnetic field at the interface $z = 0$ and making use of the relations between the field components [Eqs. (11)-(14)]. The continuity of the tangential (normal) component of the electric field (magnetic induction) imply that $q_1 = q_2 \equiv q$, $E_{1,x(y)} = E_{2,x(y)}$ and $B_{1,z} = B_{2,z}$. The discontinuity of the tangential component of the magnetic field yields

$$\frac{1}{\mu_1} B_{1,y} - \frac{1}{\mu_2} B_{2,y} = -\sigma_{xx} E_{1,x} - \sigma_{xy} E_{1,y}, \quad (16)$$

$$\frac{1}{\mu_1} B_{1,x} - \frac{1}{\mu_2} B_{2,x} = \sigma_{yx} E_{1,x} + \sigma_{yy} E_{1,y}, \quad (17)$$

where $\sigma_{\alpha\beta} \equiv \sigma_{\alpha\beta}(\mathbf{q}, \omega)$ [$\alpha, \beta = x, y$] denotes the dynamical conductivity of graphene,

$$\sigma_{\alpha\beta}(\mathbf{q}, \omega) = \frac{J_{s,\alpha}(\mathbf{q}, \omega)}{E_{s,\beta}(\mathbf{q}, \omega)}, \quad (18)$$

and relates the Fourier transforms of the surface current, $J_{s,\alpha}(\mathbf{q}, \omega)$, and that of the electric field, $E_{s,\beta}(\mathbf{q}, \omega)$, at $z = 0$. The use of the local limit of the conductivity $\sigma_{L(H)}(\mathbf{q} = 0, \omega)$ is justified whenever the wave vectors of interest are much smaller than the inverse of typical length scales. In the absence of a magnetic field, the local limit is justified for $|\mathbf{q}| \ll a_0^{-1}$, with a_0 being the carbon-carbon distance in graphene, whereas for a quantizing magnetic field the condition changes to $|\mathbf{q}| \ll l_B^{-1}$, where l_B denotes the magnetic length (see Appendix B).

Combining the above results, it is straightforward to obtain the general dispersion relation

$$\frac{i\omega}{\kappa_1} \epsilon_1 \left[\left(1 + \frac{\kappa_1 \epsilon_2}{\kappa_2 \epsilon_1} \right) - \sigma_L \frac{\kappa_1}{i\omega \epsilon_1} \right] \times \\ \times \left[\sigma_L - \left(\frac{\kappa_1}{\mu_1} + \frac{\kappa_2}{\mu_2} \right) \frac{1}{i\omega} \right] = \sigma_H^2. \quad (19)$$

In order to obtain the above expression, we have invoked rotational symmetry and use the notation employed in the main text: $\sigma_L \equiv \sigma_{xx}$ and $\sigma_H \equiv \sigma_{xy}$. Setting $\epsilon_1(\mu_1) = \epsilon_2(\mu_2) \equiv \epsilon(\mu)$ (and hence $\kappa_1 = \kappa_2 \equiv \kappa$) leads to the Eq. (2) in the main text. We remark that the term with σ_H is negligible for most choices of parameters. We have verified that only near at the QTE/MPP transitions, where $\sigma_L'' \simeq 0$, the Hall conductivity σ_H provides a small correction to the spectrum.

VII. APPENDIX B: MAGNETO-OPTICAL CONDUCTIVITY OF GRAPHENE

Within the Dirac-cone approximation,[8] and modeling the effect of disorder by an energy broadening function, the magneto-optical conductivity of graphene at Fermi energy E_F and temperature T assumes the simple form[18, 19]

$$\sigma_{L(H)}(\omega, B) = g_s g_v \times \frac{e^2}{4\hbar} \times \\ \times \sum_{n \neq m} \frac{\Xi_{L(H)}^{nm}}{i\Delta_{nm}} \frac{n_F(E_n) - n_F(E_m)}{\hbar\omega + \Delta_{nm} + i\Gamma_{nm}(\omega)}, \quad (20)$$

where $g_{s(v)} = 2$ is the spin (valley) degeneracy factor of graphene, $n_F(E) = 1/[1 + e^{(E-E_F)/k_B T}]$ stands for the Fermi distribution function, $\Gamma_{nm}(\omega)$ is the LL broadening, $\Delta_{nm} = E_n - E_m$, with LL energies E_n given by

$$E_n = \text{sign}(n) [\hbar v_F / l_B] \sqrt{2|n|}, \quad (21)$$

with l_B denoting the magnetic length, $l_B \equiv \sqrt{\hbar/(eB)}$, $v_F \simeq 10^6$ m/s is the Fermi velocity, and

$$\Xi_L^{nm} = \frac{\hbar^2 v_F^2}{l_B^2} (1 + \delta_{m,0} + \delta_{n,0}) \delta_{|m|-|n|, \pm 1}, \quad (22)$$

$$\Xi_H^{nm} = i \Xi_L^{nm} (\delta_{|m|,|n|-1} - \delta_{|m|-1,|n|}). \quad (23)$$

The use of the low-energy (Dirac-cone approximation) theory to compute $\sigma_{L(H)}$ assumes an infinite sea of negative energy states, and thus requires a cutoff $|n|, |m| \leq N_{\text{cut}}$ in Eq. (20). The respective cutoff energy $E_{N_{\text{cut}}}$ is of the order of graphene's bandwidth. Results are largely insensitive to the precise value chosen for the cutoff; in our numerical calculations we have considered $E_{N_{\text{cut}}} = 3$ eV.

The magneto-optical conductivity of graphene has two types of terms: i) intraband contributions corresponding to transitions within the same Dirac cone (i.e., $n = m \pm 1$), and ii) interband transitions that couple the valence and conduction Dirac cones (i.e., $n = -m \pm 1$). Transitions involving the zero energy LL (e.g., $n = 0 \rightarrow n = 1$) need to be considered separately because this LL state contains electrons and holes. Here, for convenience, we classify the transitions involving the zero energy LL as interband-like.

The general expression Eq. (20) can be put into a more useful form by separating interband and intraband contributions (with the proviso made in the previous paragraph). For sake of simplicity, we assume $T = 0$ and $E_F \geq 0$ [the conductivity for holes can be obtained using the symmetry relations: $\sigma_L(-E_F) = \sigma_L(E_F)$ and $\sigma_H(-E_F) = -\sigma_H(E_F)$]. We denote the number of occupied electron LLs with $E > 0$ by N_F , that is, $N_F = \text{int}[(E_F/E_1)^2] \geq 0$. Intraband transitions ($n = N_F \rightarrow n = N_F + 1$) involve an energy difference of $\Delta_{\text{intra}} = \sqrt{2}\hbar v_F/l_B(\sqrt{N_F+1} - \sqrt{N_F})$. Its contribution to the conductivity dominates at small frequencies where most of the spectral weight is concentrated around $\omega = \Delta_{\text{intra}}/\hbar$. The intraband (semi-classical) conductivity consists of a single term in the summation Eq. (20) and reads

$$\sigma_L^{(\text{intra})} = \frac{2e^2}{h} \frac{\hbar^2 v_F^2}{l_B^2 \Gamma \Delta_{\text{intra}}} \frac{1 - i\hbar\omega/\Gamma}{(1 - i\hbar\omega/\Gamma)^2 + \Delta_{\text{intra}}^2/\Gamma^2}, \quad (24)$$

$$\sigma_H^{(\text{intra})} = -\frac{2e^2}{h} \frac{\hbar^2 v_F^2}{l_B^2 \Gamma^2} \frac{1}{(1 - i\hbar\omega/\Gamma)^2 + \Delta_{\text{intra}}^2/\Gamma^2}. \quad (25)$$

According to our classification the latter equations are valid for $N_F \neq 0$, otherwise there is no intraband contribution. Note that for high Fermi energy/low magnetic field, one recovers the familiar semi-classical Drude conductivity [Eqs. (33)-(34)], since the cyclotronic gap Δ_{intra} tends to the cyclotron energy $\hbar\omega_c$ when many levels are occupied, $N_F \gg 1$. [19]

Interband terms dominate at frequencies close or above the interband threshold, $\omega = 2E_F/\hbar$. These transitions involve the energy difference energy $\Delta_n \equiv \sqrt{2}\hbar v_F/l_B(\sqrt{n+1} + \sqrt{n})$, with $n \geq N_F$. Its contribution to the magneto-optical conductivity reads

$$\sigma_L^{(\text{inter})} = \frac{2e^2}{h} \frac{\hbar^2 v_F^2}{l_B^2} \sum_{n=N_F}^{N_{\text{cut}}} (1 + \delta_{n,0})(2 - \delta_{n,N_F}) \times \frac{1}{\Gamma \Delta_n} \frac{1 - i\hbar\omega/\Gamma}{(1 - i\hbar\omega/\Gamma)^2 + \Delta_n^2/\Gamma^2}, \quad (26)$$

$$\sigma_H^{(\text{inter})} = -\frac{2e^2}{h} \frac{\hbar^2 v_F^2}{l_B^2 \Gamma^2} \frac{1 + \delta_{N_F,0}}{(1 - i\hbar\omega/\Gamma)^2 + \Delta_{N_F}^2/\Gamma^2}. \quad (27)$$

VIII. APPENDIX C: SEMI-CLASSICAL DISPERSION

We now derive an approximate formula for the semi-classical MPP dispersion. The first step is to solve Eq. (2) for $\kappa(\Omega)$; we obtain

$$\kappa(\Omega) = \frac{X(\Omega) \pm \sqrt{4f(\Omega)g(\Omega) + X(\Omega)^2}}{2f(\Omega)}, \quad (28)$$

with the notation,

$$f(\Omega) = \frac{i}{2\Omega\epsilon} \sigma_L(\Omega, B), \quad (29)$$

$$g(\Omega) = \frac{i\Omega\mu}{2} \sigma_L(\Omega, B), \quad (30)$$

$$X(\Omega) = -1 + f(\Omega)g(\Omega) - \frac{\mu}{4\epsilon} \sigma_H^2(\Omega, B). \quad (31)$$

The sign in the numerator in Eq. (28) must be chosen according to the requirements necessary to obtain a physical solution (Appendix A). The function $q(\omega)$ then follows from Eq. (15),

$$q(\Omega) = \sqrt{\kappa(\Omega)^2 + \epsilon_r \Omega^2/c^2}, \quad (32)$$

where ϵ_r denotes the relative permittivity of the dielectric medium surrounding graphene. In order to proceed, we neglect the effect of interband transitions and approximate Eqs. (24)-(25) by its semi-classical analogue, [19]

$$\sigma_L = \frac{e^2}{h} \frac{2|E_F|}{\Gamma} \frac{1 - i\hbar\Omega/\Gamma}{(1 - i\hbar\Omega/\Gamma)^2 + \Delta^2/\Gamma^2}, \quad (33)$$

$$\sigma_H = -\frac{e^2}{h} \frac{2E_F}{\Gamma} \frac{\Delta/\Gamma}{(1 - i\hbar\Omega/\Gamma)^2 + \Delta^2/\Gamma^2}, \quad (34)$$

where $\Delta = \hbar v_F^2 B/|E_F|$ is the intraband cyclotron gap. The semi-classical expressions have the advantage of simplifying the notation and introducing the cyclotron energy which is more used in the literature (albeit less accurate) than the intraband gap, Δ_{intra} . The crucial point to derive a compact expression for the dispersion relation is to note that for typical frequencies \sim THz and $\Gamma \sim 0.01$ eV, we have $f \times g \ll X^2$, and therefore the expression for $\kappa(\Omega)$ can be approximated by

$$\kappa(\Omega) \simeq \frac{X(\Omega)}{f(\Omega)}, \quad (35)$$

where we have chosen the appropriate sign in Eq. (28). (Note that the other solution has $\kappa(\Omega) \simeq 0$ and would correspond to a QTE mode.) Taking the square of both sides of Eq. (35), substituting the conductivity tensor components [Eqs. (33)-(34)] into $X(\Omega)$, and employing a series expansion for small $\Delta/\hbar\Omega$ and $\Gamma/\hbar\Omega$, we obtain,

$$q'^2 + q''^2 \simeq \epsilon_r \frac{\Omega^2}{c^2} + \left(\frac{2\pi\epsilon\hbar\Omega}{E_F e^2} \right)^2 (\hbar^2 \Omega^2 - 2\Delta^2), \quad (36)$$

where we have kept the terms up to second order in the small parameters, and assumed $\hbar\Omega/E_F \gg g_0 \mathcal{Z} \simeq 0.1$ (with $g_0 \equiv 2e^2/h$ denoting the quantum of conductance). We remark that these approximations are consistent with the small wavelength limit, for which $\hbar\Omega$ is typically larger than other energy scales. Assuming negligible damping $q'' \ll q'$, more precisely, requiring

$$\Gamma \ll \frac{E_F^2 e^4 q'^2}{\epsilon^2 \hbar^3 \Omega^3}, \quad (37)$$

and taking $q' \gg \Omega/c$ (non-retarded regime) in Eq. (36), we arrive at the final result,

$$q' \approx \frac{2\pi\epsilon\hbar\Omega}{|E_F|e^2} \sqrt{\hbar^2\Omega^2 - 2\Delta^2}. \quad (38)$$

The magneto-plasmon spectrum [Eq. (4)] follows immediately by expanding the latter expansion in the small parameter $\Delta/\hbar\Omega$.

-
- [1] T. W. Ebbesen, H. J. Lezec, H. F. Ghaemi, T. Thio, and P. A. Wolf, *Nature* **391**, 667 (1998).
- [2] S. A. Maier, *Plasmonics: Fundamentals and Applications*, Springer (2007).
- [3] A. Vakil, and N. Engheta, *Science* **332**, 1291 (2011).
- [4] F. Schedin, E. Lidorikis, A. Lombardo, V. G. Kravets, A. K. Geim, A. N. Grigorenko, K. S. Novoselov, and A. C. Ferrari, *ACS Nano* **4**, 5617 (2010).
- [5] T. J. Echtermeyer, L. Britnell, P. K. Jasnós, A. Lombardo, R. V. Gorbachev, A. N. Grigorenko, A. K. Geim, A. C. Ferrari, and K. S. Novoselov, *Nature Communications* **2**, 458 (2011).
- [6] L. Ju, B. Geng, J. Horng, C. Girit, M. C. Martin, Z. Hao, H. A. Bechtel, X. Liang, A. Zettl, Y. R. Shen, and F. Wang, *Nature Nanotechnology* **6**, 630 (2011).
- [7] Z. Fei, G. O. Andreev, W. Bao, and *et al.*, *Nano Lett.* **11**, 4701 (2011).
- [8] A. H. Castro Neto, F. Guinea, N. M. R. Peres, K. S. Novoselov, and A. K. Geim, *Rev. Mod. Phys.* **81**, 109 (2009).
- [9] Yu. V. Bludov, M. I. Vasilevskiy, and N. M. R. Peres, *EPL* **92**, 68001 (2010).
- [10] M. Jablan, H. Buljan, and M. Soljačić, *Phys. Rev. B* **80**, 245435 (2009).
- [11] F. H. L. Koppens, D. E. Chang, and F. J. G. de Abajo, *Nano Lett.* **11**, 3370 (2011).
- [12] K. W. Chiu, and J. J. Quinn, *Phys. Rev. B* **9**, 4724 (1974).
- [13] I. V. Kukushkin, V. M. Muravev, J. H. Smet, M. Hauser, W. Dietsche, and K. von Klitzing, *Phys. Rev. B* **73**, 113310 (2006).
- [14] Usually experiments are done with graphene on top of a substrate such as SiO₂ (see e.g., Ref. [7]). The presence of two distinct dielectrics can be accounted for letting $\epsilon \rightarrow (\epsilon_1 + \epsilon_2)/2$, where $\epsilon_{1(2)}$ concerns with the top (bottom) dielectric. This prescription is accurate in the non-retarded regime $q' \gg \Omega/c$; for the exact dispersion relation we refer to Appendix I.
- [15] W. L. Barnes, A. Dereux, and T. W. Ebbesen, *Nature (London)* **424**, 824 (2003).
- [16] S. A. Mikhailov, and K. Ziegler, *Phys. Rev. Lett.* **99**, 016803 (2007).
- [17] Q. Bao, H. Zhang, B. Wang, Z. Ni, C. H. Y. X. Lim, Y. Wang, D. Y. Tang, and K. P. Loh, *Nature Photonics* **5**, 411(2011).
- [18] V.P. Gusynin, S.G. Sharapov, and J.P. Carbotte, *J. Phys.: Condens. Matter* **19**, 026222 (2007).
- [19] A. Ferreira, J. Viana-Gomes, Yu. V. Bludov, V. Pereira, N. M. R. Peres, A. H. Castro Neto, *Phys. Rev. B* **84**, 235410 (2011).
- [20] J. M. Dawlaty, S. Shivaraman, M. Chandrashekar, F. Rana, and M. G. Spencer, *Appl. Phys. Lett.* **92**, 042116 (2008).
- [21] M. Breusing, S. Kuehn, T. Winzer, E. Malić, F. Milde, N. Severin, J. P. Rabe, C. Ropers, A. Knorr, and T. Elsaesser, *Phys. Rev. B* **83**, 153410 (2011).
- [22] J. Horng, C.-F. Chen, B. Geng, C. Girit, Y. Zhang, Z. Hao, H. A. Bechtel, M. Martin, A. Zettl, M. F. Crommie, Y. R. Shen, and F. Wang, *Phys. Rev. B* **83**, 165113 (2011).
- [23] A. Pound, J. P. Carbotte, and E. J. Nicol, *EPL* **94**, 57006 (2011).
- [24] D. C. Bardos, and N. E. Frankel, *Phys. Rev. B* **49**, 4096 (1994).
- [25] F. Stern, *Phys. Rev. Lett.* **18**, 546 (1967).
- [26] K. W. K. Shung, *Phys. Rev. B* **34**, 979 (1986).
- [27] Numerical analysis show that the expression for $\Omega(0)$ is valid for $B > B_c$ in a wide range of E_F, B values with Γ of order of the remaining energy scales.